Iranian Journal of Science & Technology, Transaction B, Engineering, Vol. 31, No. B1, pp 65-80
Printed in The Islamic Republic of Iran, 2007
© Shiraz University

GROUND VIBRATION TEST (GVT) AND CORRELATION ANALYSIS OF AN AIRCRAFT STRUCTURE MODEL*

M. SALEHI** AND S. ZIAEI-RAD

Dept. of Mechanical Engineering, Isfahan University of Technology, Isfahan, I. R. of Iran
Email: szrad@cc.iut.ac.ir

Abstract– Ground Vibration Test (GVT) is one of the standard tests used for designing new aircraft. In this paper, GVT was carried out on an aircraft structure model by the phase separation method. In order to obtain more accurate results, the structure was excited by hammer, random and sine excitations. The results were then used to extract the modal parameters, i.e. natural frequencies, modal damping factors and mode shapes. Extraction algorithms were based on multi-degree of freedom (MDoF) methods where several FRFs are analyzed simultaneously. Correlation between different test techniques was also investigated. Next, a finite element model of the structure was constructed and the theoretical modal analysis results have been compared with experimental ones. The test results obtained from the phase separation technique were also compared with a similar test carried out on the same structure by the phase resonance method. Finally, a cylindrical mass was added to the right tail wing of the model. A new set of modal tests was carried out to investigate the effect of unsymmetry on the modal properties of the structure.

Keywords– Ground Vibration Test, modal analysis, modal testing, aircraft structure

1. INTRODUCTION

Ground Vibration Test (GVT) plays an important role in the certification process of any new or extensively modified aircraft. GVT results provide experimental data which are essential in flutter prediction as well as to validate and update analytical aircraft models. The GVT of an aircraft structure determines its natural frequencies, normal mode shapes and generalized parameters (mass, stiffness and damping) over a specified frequency bandwidth.

There are several methods for carrying out the GVT. These can be mainly classified into two groups, namely phase resonance and phase separation. The phase resonance method requires an appropriate exciter configuration to be applied for each normal mode in order to compensate for internal damping forces. In this case, the structure vibrates solely in the respective normal mode.

On the other hand, the phase separation method uses single or multiple broadband excitation signals to excite the structure so that all desired modes are excited simultaneously. Resulting Frequency Response Function (FRF) measurements contain the required information. Curve fitting algorithms are then applied to extract the modal data from the measured FRFs. In contrast to phase resonance that separates the modes physically, the phase separation method separates the modes of the structure mathematically by use of some curve fitting algorithms.

Following a series of previous Round Robin surveys on GVT held in the early 60s [1] and late 70s [2], a structures action group called GARTEUR was initiated in April 1995, with the major objective to compare a number of current measurement and identification techniques applied to a common structure

*Received by the editors December 8, 2005; final revised form January 2, 2007.
**Corresponding author

Archive of SID

www.SID.ir

[3]. A testbed (see Fig. 1) was designed and manufactured by ONERA (France) and investigated by various companies, research centers and universities [4]. The results obtained from the testing of the 12 laboratories on this structure are presented in the paper by Balmes and Wright [5].

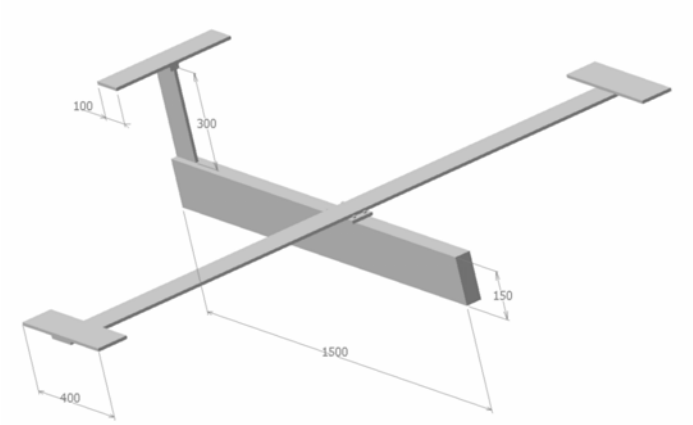

Fig. 1. Schematic of the aircraft structure model

As a next step, different FE models of the test structure were updated based on the measured FRFs by different groups. Goge and Link [6] applied the classical inverse sensitivity approach to minimize the deviations between analytical and measured modal data. Mares *et al.* [7] updated their FE model using sensitivity analysis. They claimed that the updating process could accurately reproduce test data by selecting the updating parameters based on physical understanding, scrutiny of the mode shapes and sensitivity calculations. Bohle and Fritzen [8] updated a plate model of the structure by minimizing the residuals between theoretical and experimental natural frequencies and mode shapes. Thonon and Golinval [9] generated a low-order finite element model of the structure and updated it based on the computation of the residual strain energy due to errors in the constitutive equations. D'Ambrogio and Redolent [10] used an extension of the antiresonance-based model updating method to reduce the difference between measured and analytical FRFs. Ziaei-Rad [11] used different optimization techniques for model updating of rotating and non-rotating structures. The use of both deterministic and stochastic optimization methods was investigated in order to minimize the difference between analytical and measured data. In a separate paper, Ziaei-Rad [12] applied the deterministic FRF based updating technique to an industrial radial flow impeller. The experimental results obtained from impact testing and the laser Doppler vibrometer was compared with the results from the FE model.

This paper describes test procedure, parameter extraction, finite element modeling and correlation analysis between different test methods and FE results. Our results, mainly based on phase separation, were also compared with those obtained by DLR Germany using phase resonance on the GARTUER structure [4, 13]. The effect of modification on the structure was also investigated using both experimental and analytical techniques.

2. THE TEST STRUCTURE

The testbed has been designed and manufactured to be representative of typical aircraft structures (Fig. 1). For this purpose, the following design requirements were proposed:

- General shape: beam assembly representing a fuselage with wings and tail
- Damping treatment by means of constrained viscoelastic layers in order to get damping coefficients as high as those encountered on a real aircraft
- No specific non-linear elements

Archive of SID
www.SID.ir

- Very low frequency suspension as part of the testbed in order to eliminate the surroundings effect
- The testbed presents three very close modes in order to simulate the difficulty encountered on an aircraft

3. THEORY

a) Phase separation

There are two major methods in modal data extraction from measurement data namely, Single Degree of Freedom (SDoF) and MDoF methods. Many algorithms have been developed in these two categories both in time and frequency domain [14]. SDoF methods are not well suited for dealing with close modes. Since there are three close modes in the test results, Rational Fraction Polynomials (RFP), which is an MDoF method, has been adopted through the study to extract the modal parameters.

In the rational fraction formulation, an error function is established in a way that the resulting system of equations is linear. Because the resulting linear system of equations involves ill-conditioned matrices, the gradient method is used to minimize the error function.

The receptance FRF for a linear system with N degrees of freedom and structural damping can be modeled with the following partial fraction equation [14]:

$$H(\omega)=\sum_{r=1}^{N}\frac{A_r+i\omega B_r}{\omega_r^2-\omega^2+i\eta_r\omega_r{}^2} \tag{1}$$

Where A_r and B_r are constants and η_r is the damping ratio. Equation (1) can also be expressed in rational fraction form as follows:

$$H(\omega)=\frac{\sum_{k=0}^{2N-1}a_k(i\omega)^k}{\sum_{k=0}^{2N}b_k(i\omega)^k} \tag{2}$$

The difference between the analytical FRF, $H(\omega)$, and the experimental one, $H_e(\omega)$, is the error function and is given by:

$$e_j=\frac{\sum_{k=0}^{2N-1}a_k(i\omega)^k}{\sum_{k=0}^{2N}b_k(i\omega)^k}-H_e(\omega_j) \tag{3}$$

The error function is linearized by working with the following modified error function:

$$e'_j=e_j\sum_{k=0}^{2N}b_k(i\omega_j)^k \tag{4}$$

Making $b_{2N}=1$ leads to

$$e'_j=\sum_{k=0}^{2N-1}a_k(i\omega_j)^k-H_e(\omega_j)\left[\sum_{k=0}^{2N-1}b_k(i\omega_j)^k+(i\omega_j)^{2N}\right] \tag{5}$$

Archive of SID
www.SID.ir

An error vector is defined for all the L measured frequencies

$$\{E\} = \begin{Bmatrix} e'_1 \\ e'_2 \\ : \\ e'_L \end{Bmatrix} \tag{6}$$

Equation (5) can then be written in the matrix form as:

$$\{E\} = \begin{bmatrix} 1 & (i\omega_1) & (i\omega_1)^2 & .. & (i\omega_1)^{2N-1} \\ 1 & (i\omega_2) & (i\omega_2)^2 & .. & (i\omega_2)^{2N-1} \\ : & : & : & : & : \\ 1 & (i\omega_L) & (i\omega_L)^2 & .. & (i\omega_L)^{2N-1} \end{bmatrix} \begin{Bmatrix} a_0 \\ a_1 \\ : \\ a_{2N-1} \end{Bmatrix} -$$
$$\begin{bmatrix} H_e(\omega_1) & H_e(\omega_1)(i\omega_1) & .. & H_e(\omega_1)(i\omega_1)^{2N-1} \\ H_e(\omega_2) & H_e(\omega_2)(i\omega_2) & .. & H_e(\omega_2)(i\omega_2)^{2N-1} \\ : & : & : & : \\ H_e(\omega_L) & H_e(\omega_L)(i\omega_L) & .. & H_e(\omega_L)(i\omega_L)^{2N-1} \end{bmatrix} \begin{Bmatrix} b_0 \\ b_1 \\ : \\ b_{2N-1} \end{Bmatrix} - \begin{Bmatrix} H_e(\omega_1)(i\omega_1)^{2N} \\ H_e(\omega_2)(i\omega_2)^{2N} \\ : \\ H_e(\omega_L)(i\omega_L)^{2N} \end{Bmatrix} \tag{7}$$

or

$$\underset{(L\times 1)}{\{E\}} = \underset{(L\times 2N)}{[P]} \underset{(2N\times 1)}{\{a\}} - \underset{(L\times 2N)}{[T]} \underset{(2N\times 1)}{\{b\}} - \underset{(L\times 1)}{\{W\}} \tag{8}$$

The equation that will be minimized with the gradient method is the squared error function J, i.e.:

$$J = \{E^*\}^T \{E\} \tag{9}$$

Where * indicates the complex conjugate. Substituting Eq. (8) in (9) leads to:

$$J = \{a\}^T \,\mathrm{Re}\left([P^*]^T [P]\right)\{a\} + \{b\}^T \,\mathrm{Re}\left([T^*]^T [T]\right)\{b\} + \{W^*\}^T \{W\} -$$
$$2\{a\}^T \,\mathrm{Re}\left([P^*]^T [T]\right)\{b\} - 2\{a\}^T \,\mathrm{Re}\left([P^*]^T [W]\right) + 2\{b\}^T \,\mathrm{Re}\left([T^*]^T [W]\right) \tag{10}$$

This is an equation with ill-conditioned matrices and should be solved by the gradient method in order to minimize the error function. To obtain the initial estimate needed for the gradient method, one can use the least square technique.

Taking the derivatives of Eq. (10) with respect to $\{a\}$ and $\{b\}$, equating them to zero gives the following system of equations:

$$\mathrm{Re}\left([P^*]^T [P]\right)\{a\} - \mathrm{Re}\left([P^*]^T [T]\right)\{b\} - \mathrm{Re}\left([P^*]^T \{W\}\right) = \{0\}$$
$$\mathrm{Re}\left([T^*]^T [T]\right)\{b\} - \mathrm{Re}\left([T^*]^T [P]\right)\{a\} - \mathrm{Re}\left([T^*]^T \{W\}\right) = \{0\} \tag{11}$$

or

$$\begin{bmatrix} [Y] & [X] \\ [X]^T & [Z] \end{bmatrix} \begin{Bmatrix} \{a\} \\ \{b\} \end{Bmatrix} = \begin{Bmatrix} \{G\} \\ \{F\} \end{Bmatrix} \tag{12}$$

Archive of SID

www.SID.ir

where

$$\begin{aligned}
[Y] &= \mathrm{Re}\left(\left[P^*\right]^T[P]\right)\\
[X] &= -\mathrm{Re}\left(\left[P^*\right]^T[T]\right)\\
[Z] &= \mathrm{Re}\left(\left[T^*\right]^T[T]\right)\\
\{G\} &= \mathrm{Re}\left(\left[P^*\right]^T\{W\}\right)\\
\{F\} &= -\mathrm{Re}\left(\left[T^*\right]^T\{W\}\right)
\end{aligned} \tag{13}$$

These equations are first solved to find the initial values $\{a\}$ and $\{b\}$ which are later used to evaluate the gradient. The gradients are

$$\begin{aligned}
&\mathrm{Re}\left(\left[P^*\right]^T[P]\right)\{a\} - \mathrm{Re}\left(\left[P^*\right]^T[T]\right)\{b\} - \mathrm{Re}\left(\left[P^*\right]^T\{W\}\right) = \{M\}\\
&\mathrm{Re}\left(\left[T^*\right]^T[T]\right)\{b\} - \mathrm{Re}\left(\left[T^*\right]^T[P]\right)\{a\} - \mathrm{Re}\left(\left[T^*\right]^T\{W\}\right) = \{N\}
\end{aligned} \tag{14}$$

Where $\{M\}$ and $\{N\}$ are gradient vectors with respect to $\{a\}$ and $\{b\}$. The total gradient vector is

$$\{V\} = \begin{Bmatrix} M \\ N \end{Bmatrix} \tag{15}$$

The gradient vector direction is calculated to move in the direction where the function is minimized. The gradient vector direction is

$$\{S\} = \frac{-\{V\}}{\|\{V\}\|} \tag{16}$$

Finally, the new coefficients are

$$\begin{Bmatrix} a \\ b \end{Bmatrix}^{new} = \begin{Bmatrix} a \\ b \end{Bmatrix}^{old} + \{S\} \tag{17}$$

After obtaining the coefficients of rational fraction Eq. (2), modal parameters can be calculated. The poles of the denominator polynomial contain the values of the natural frequencies and damping ratios. In order to calculate residues, the rational fraction is expanded in a partial fraction equation and the numerator becomes a pair of complex conjugate constants called residues.

b) Phase resonance

Generally, the equation of motion of an N degrees of freedom system can be written as follows:

$$[M]\{\ddot{x}\} + [C]\{\dot{x}\} + [K]\{x\} = \{F\} \tag{18}$$

where [M], [C] and [K] matrices represent mass, damping and stiffness respectively. For most practical analysis, however, a proportional damping behavior can be assumed resulting in a diagonal damping matrix. In general, these matrices have nonzero off-diagonal elements so that the N equations are coupled. The purpose of a phase resonance test is to uncouple these equations. This is accomplished by identifying

Archive of SID

www.SID.ir

the mode shapes. Phase resonance testing assumes the mode shapes, $\{\phi_n\}$, are real valued. Any arbitrary pattern of motion, x is a linear combination of N mode shapes $\{\phi_n\}$, where the weighting coefficients of this summation are provided by the modal participation vector, $\{q\}$

$$\{x\} = [\{\phi\}_1 \quad ... \quad \{\phi\}_n \quad ... \quad \{\phi\}_N]\{q\} = [\phi]\{q\} \tag{19}$$

The normal mode solution vectors have an important mathematical property termed "generalized orthogonality" with respect to mass, stiffness and damping matrices. This property can be used to diagonalize all three matrices when applied as a similarity transformation. Once the transformation is performed upon mass matrix, we have

$$[\phi]^T [M][\phi] = \begin{bmatrix} \ddots & & \\ & d_n & \\ & & \ddots \end{bmatrix} \tag{20}$$

Substituting Eq. (20) into Eq. (18) yields:

$$[\phi]^T [M][\phi]\{\ddot{q}\} + [\phi]^T [C][\phi]\{\dot{q}\} + [\phi]^T [K][\phi]\{q\} = [\phi]^T \{F\} \tag{21}$$

If mass normalization of mode shapes is done, the above equation can be rewritten as follows:

$$\begin{bmatrix} \ddots & & \\ & 1 & \\ & & \ddots \end{bmatrix}\{q\} + \begin{bmatrix} \ddots & & \\ & 2\xi_n\omega_n & \\ & & \ddots \end{bmatrix}\{\dot{q}\} + \begin{bmatrix} \ddots & & \\ & \omega_n^2 & \\ & & \ddots \end{bmatrix}\{q\} = [\phi]^T \{F\} = \{Q\} \tag{22}$$

Hence the only coupling between the resulting N equations is in the right hand side. That is, the manner in which the structure is forced determines the coupling between the normal modes in Eq. (22). The excitation of these uncoupled equations is not the physical force F directly; it is the generalized force vector $\{Q\} = [\phi]^T \{F\}$.

If the structure is excited with an array of sinusoidal forces all at the same frequency with amplitude distributions proportional to one of the mode shapes weighted by the mass matrix

$$\{F\} = \alpha[M]\{\phi\}_n \tag{23}$$

This results in a generalized force vector Q with zero values for all elements but the one corresponding to the selected mode shape as shown in Eq. (24).

$$\{Q\} = \alpha[\phi]^T [M]\{\phi\}_n = \begin{Bmatrix} 0 \\ \vdots \\ \alpha \\ \vdots \\ 0 \end{Bmatrix} \tag{24}$$

Hence the purpose of phase separation testing is to iteratively tune the distribution of applied forces until the generalized force is null for all but the mode sought.

4. EXPERIMENTAL SET-UP

Figure 2 shows a typical standard layout for the measurement system. The structure is excited under a controlled force by a shaker and the responses measured by several accelerometers in desired points. Force

Archive of SID

www.SID.ir

and acceleration signals transmitted to analyzer and FRFs are constructed by dividing output to input in each frequency step.

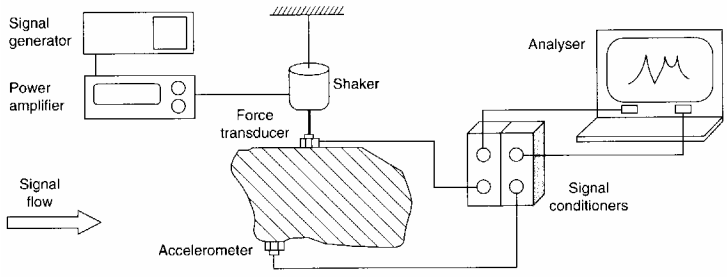

Fig. 2. A typical experimental setup

The structure has been suspended by a set of bungees to simulate the free-free boundary condition of an aircraft (Fig. 3). As shown in Fig. 4, there are 16 measurement points for accelerometer attachment. Regarding measurement directions as shown in Table 1, total measurement degrees of freedom of the testbed is 24.

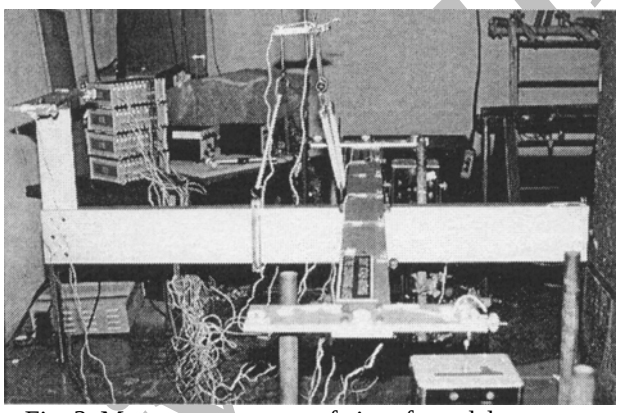

Fig. 3. Measurement setup of aircraft model structure

Table 1. Measurement points and directions

Measurement Point	Measurement Direction
1	Z
5	X, Z
8	Z
11	Z
12	X,Z
101	Z
105	X,Z
108	Z
111	Z
112	X,Z
201	X,Y,Z
205	Y
206	Z
301	X,Z
302	Y
303	X,Z

Tests have been carried out by both hammer and shaker. Random and sine signals have been used to excite the structure. All tests except the sine one were performed in a frequency range of 0-100Hz. The frequency range of the sine test was 30-60Hz. The main reason for doing the sine test was better

www.SID.ir

identification of close modes in the frequency range of 30-60HZ. Point FRFs, $H_{12z,12z}$, for sine, hammer and random excitations are shown in Fig. 5.

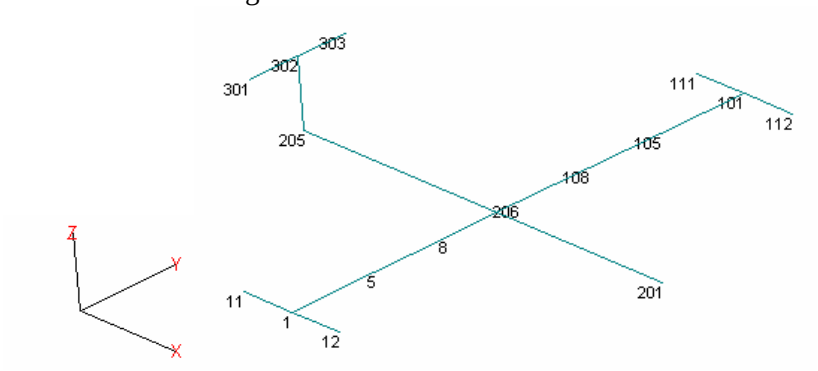

Fig. 4. Measurement points of aircraft model structure

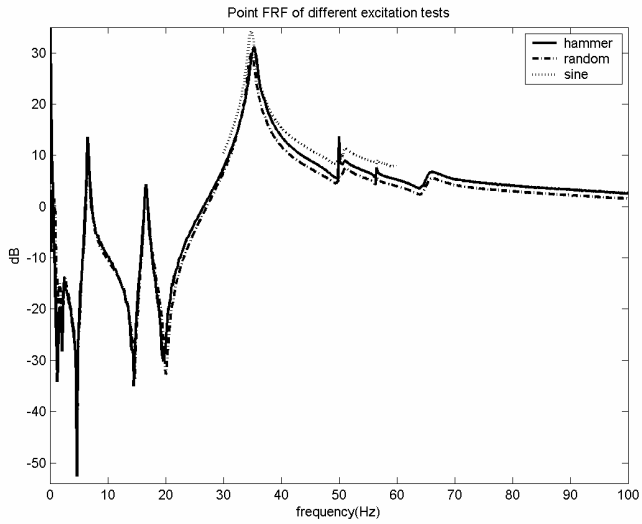

Fig. 5. Measured point FRFs of structure for different excitation techniques

5. TEST RESULTS

Modal parameters extraction was carried out by the RFP method explained in section 3a. Modal frequencies and damping coefficients obtained from hammer, random and sine tests were tabulated in Table 2. Since the sine test was carried out in the frequency range of 30-60Hz, only modes 3 to 8 could be extracted from the experimental data. Some of the mode shapes of the structure excited by different force patterns are shown in Fig. 6.

Table 2. Resonance frequencies and damping factors of the structure

Hammer			Random			Sine		
Freq No.	Freq [Hz]	Damp [%]	Freq No.	Freq [Hz]	Damp [%]	Freq No.	Freq [Hz]	Damp [%]
1	6.54	2.94	1	6.55	2.18			
2	16.56	2.70	2	16.57	2.23			
3	34.94	1.98	3	34.70	2.24	3	34.81	1.47
4	35.28	2.42	4	35.06	1.67	4	34.92	2.22
5	36.62	2.24	5	36.58	1.54	5	36.73	1.64
6	50.19	3.92	6	50.23	3.94	6	49.87	3.59
7	50.63	0.89	7	50.77	0.91	7	50.36	1.15
8	56.39	0.21	8	56.41	0.37	8	56.43	0.23
9	65.05	3.70	9	65.22	3.64			
10	69.68	0.65	10	69.92	0.64			

www.SID.ir

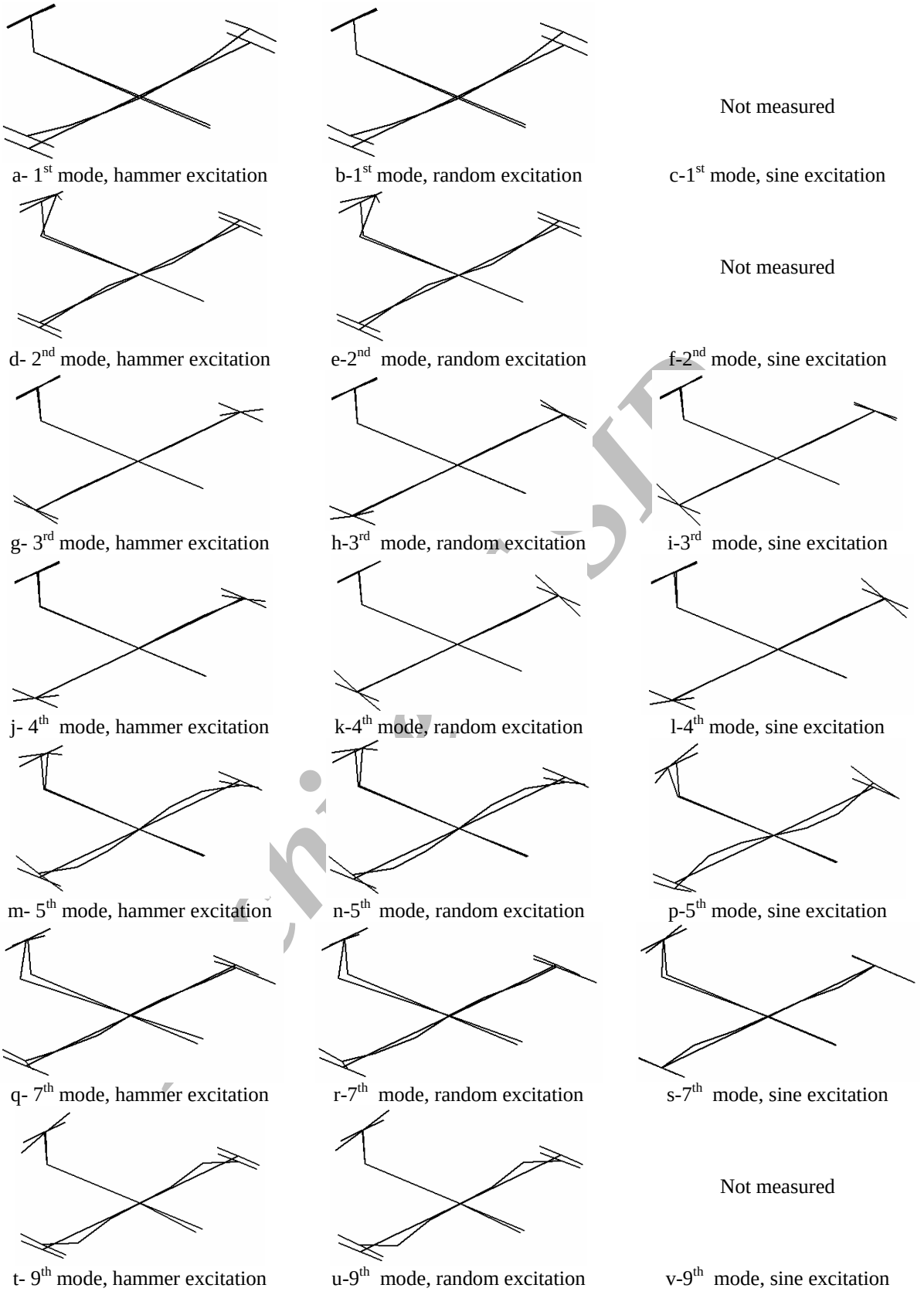

Fig. 6. Mode shapes of the structure (hammer, random and sine excitation)

There are some statistical parameters to quantify the comparison between two mode shapes. The most popular parameter is referred to as the Modal Assurance Criterion (MAC) defined as [15]:

www.SID.ir

$$MAC(\{\phi\}_1, \{\phi\}_2) = \frac{\left|\{\phi\}_1^T \{\phi\}_2\right|^2}{\left(\{\phi\}_1^T \{\phi\}_1\right)\left(\{\phi\}_2^T \{\phi\}_2\right)} \tag{25}$$

MAC values range between 0 to 1 indicating uncorrelated and full correlated mode pairs respectively. Figures 7-9 show the percentage of MAC values between mode shapes obtained from various tests, as well as a comparison of natural frequencies.

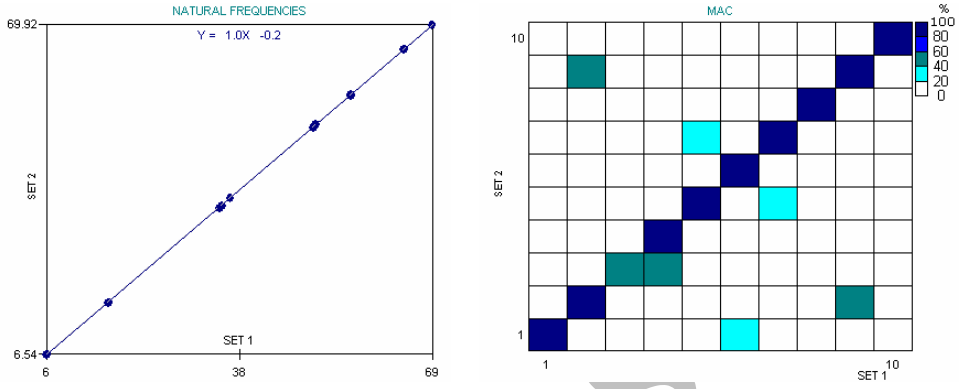

Fig. 7. Comparison of hammer versus random tests – natural frequencies and MAC

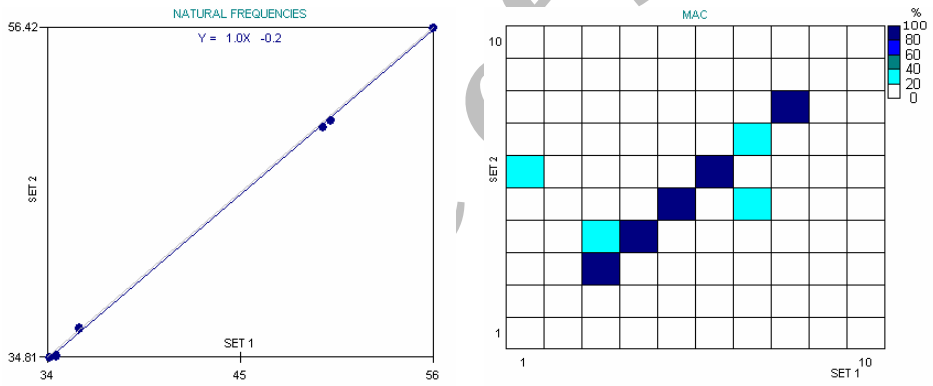

Fig. 8. Comparison of hammer versus sine tests – natural frequencies and MAC

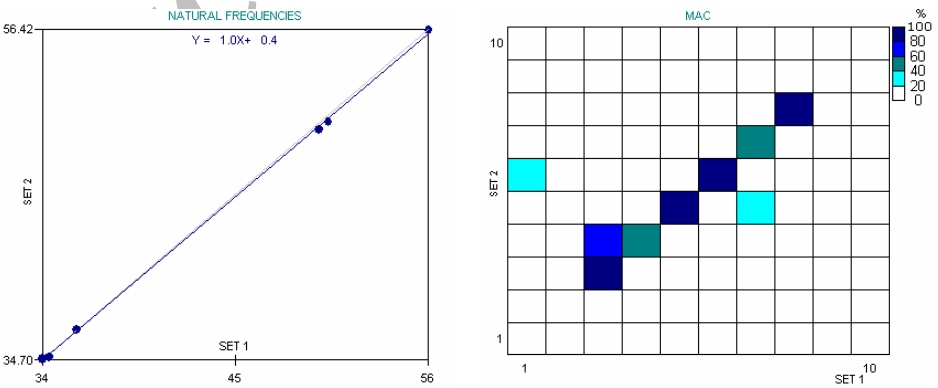

Fig. 9. Comparison of random versus sine tests–natural frequencies and MAC

Correlation between hammer and random sets was quite good (Fig. 7). However, some minor deviation can be observed between pair modes (3, 4) and (2, 9). In mode 3, wing ends vibrate anti symmetrically, while in mode 4 the motion of wing ends is symmetrical. In mode 3, the left wing end exhibits large deflections in the hammer test, but small deflections in the random test. The opposite

www.SID.ir

situation is true with the right wing end. Symmetric or anti-symmetric motions of modes have no considerable influence on the MAC values. However, large or small amplitude of deflections can greatly influence the MAC values. This is the main reason for lower MAC value (around 50%) for mode 3 from the hammer and random tests. Due to the similarity between the overall shape of modes 3 and 4, there is some correlation between these two modes (Fig. 7). The correlation between modes 2 and 9 in Fig. 7 is probably due to the fact that too few points were measured. These modes look similar, but in mode 9 the deflection of the wings is of higher order. This can also be seen from the FE model with a fine mesh (Fig. 10).

Comparing test sets hammer versus sine or random versus sine, there is some correlation between modes 3 and 4 (Figs. 8 and 9). Again, this can be explained by the similarity between these two modes. Low MAC values were calculated for mode 7. Mode 7 extracted from sine test data does not match with those extracted from random or hammer tests data. A possible reason is that there could be two very close modes on this particular frequency. One of them is excited by hammer or random tests, while the other is excited by the sine test. Note that in all three cases, only one of those modes was extracted from the measured data.

6. FINITE ELEMENT MODELING

An FE model of the structure was constructed in ANSYS (Fig. 10). The model was constructed by 32 3D beam elements. To make the FE model more accurately represent the actual structure, some modifications were applied to the initial FE model. The modification target was to increase the MAC values between theoretical modes with corresponding experimental ones. The modification was carried out by tuning the joints stiffness in both wing to fuselage, and vertical tail to horizontal tail. This was achieved by varying the stiffness and length of joint beam elements (elements A and B in Fig. 11). In addition to the above modification, two inertial elements with a mass of 0.2 kg and another with 1.6 kg mass were added to nodes 12, 112 and 302 respectively. The corrections made to the model resulted in good MAC values between analytical and experimental mode shapes. The differences in natural frequencies of both models were below 10%, except for the second mode which had an error of 21%. Analytical natural frequencies, together with experimental ones, are shown in Table 3. Some analytical mode shapes are shown in Fig. 11.

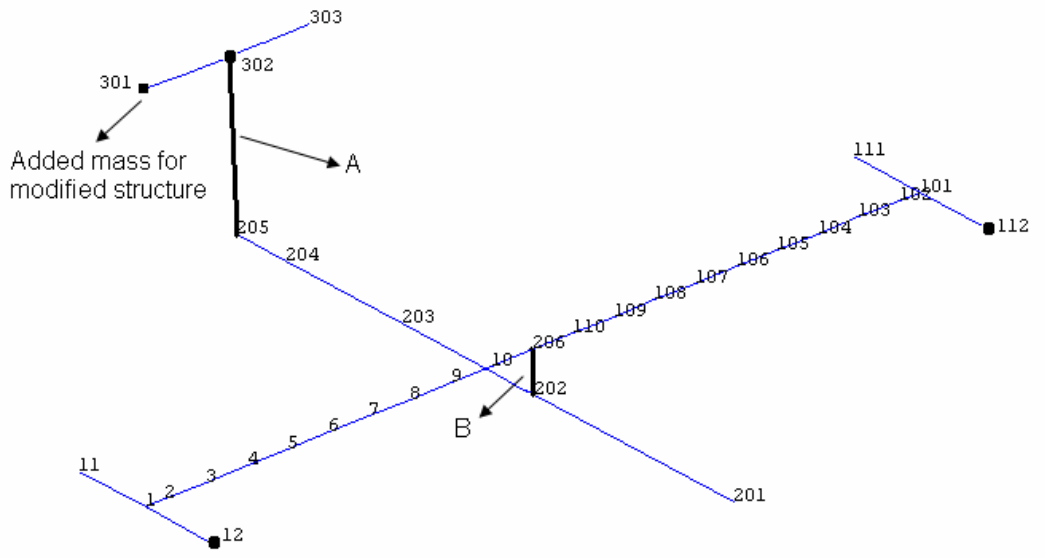

Fig. 10. The FE model of the structure

www.SID.ir

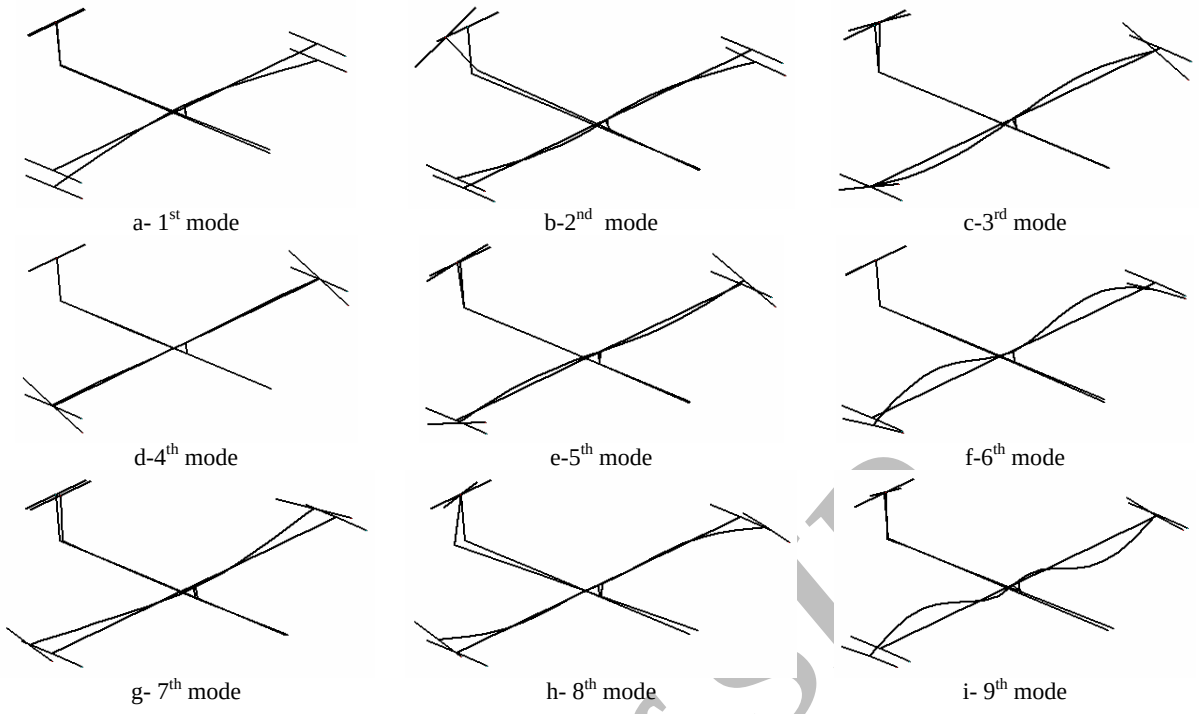

Fig. 11. Analytical mode shapes of the structure

Table 3. Natural frequencies obtained from test and FEM

Mode Number	FEM	Hammer	Random	Sine	Description
1	6.0139	6.54	6.55	N/A	First symmetric wing bending
2	12.963	16.56	16.57	N/A	Global fuselage rotation
3	31.623	34.94	34.70	34.81	Anti-symmetrical wing torsion
4	32.920	35.28	35.06	34.92	Symmetrical wing torsion
5	34.183	36.62	36.58	36.73	First anti-symmetric wing bending + anti-symmetric wing torsion
6	47.134	50.19	50.23	49.87	Second symmetric wing bending
7	55.019	50.63	50.77	50.36	Symmetric in plane bending
8	56.727	56.39	56.41	56.43	Anti-Symmetric in plane bending
9	61.911	65.05	65.22		Second anti-symmetric wing bending
10	63.863	69.68	69.92		Vertical tail torsion

MAC values of the hammer test versus FEM, as shown in Fig.12, are satisfactory. There is a mode pairing problem between modes 7 and 8. This may be due to the fact that these modes mainly occur in the xy plane where fewer transducers (See Table 1) were installed to measure the responses. Visual inspection of 7th experimental and 8th analytical modes clearly verifies the similarity between these two modes. For the sake of brevity, the correlation between FEM and other test data sets are not reported here.

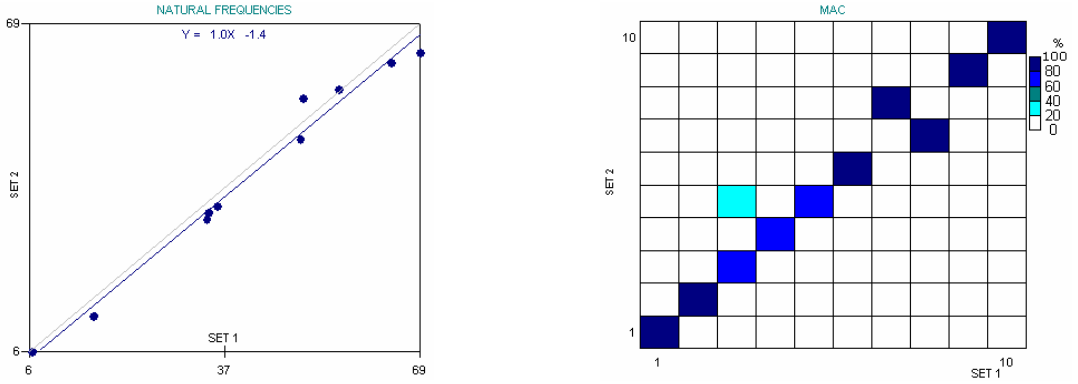

Fig.12. MAC values of hammer test versus FEM

Archive of SID
www.SID.ir

7. COMPARISON BETWEEN PHASE RESONANCE AND PHASE SEPARATION RESULTS

Vibration tests were carried out on the same structure in DLR Germany by the phase resonance method [13, 14]. In order to ensure that these two techniques are of the same accuracy, test data reported by DLR were used against those from our test results. A comparison between phase separation and phase resonance methods indicates good agreement between these two test methods. A frequency diagram, together with the corresponding MAC table, is shown in Fig. 13.

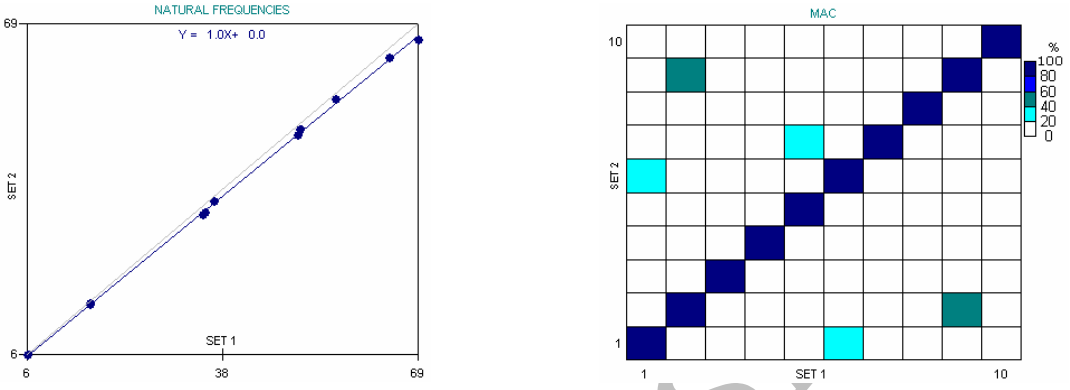

Fig. 13. MAC values of hammer test versus DLR results

8. MODIFIED STRUCTURE CASE

To study the effect of structural unsymmetry on extracted modes, a modification was done on the real structure. The modification was to add a cylindrical mass of 0.94 kg to node 301 (See Fig. 10). Inertial properties of the cylinder are tabulated in Table 4.

Table 4. Inertial properties of added mass

m	I_{xx}	I_{yy}	I_{zz}
$0.94kg$	$3.3683\times10^{-4}kg.m^4$	$3.3683\times10^{-4}kg.m^4$	$4.23\times10^{-4}kg.m^4$

Tests were carried out again on the structure for this new case. The structure was excited by both hammer and random signals. The measured FRFs were almost identical and therefore the results from excitation by hammer are reported hereafter. Again, modal analysis was carried out on the data stored in the analyzer. A modified FE model was also constructed and solved to obtain the theoretical modal parameters. Table 5 shows theoretically and experimentally extracted natural frequencies of the modified structure. For better visualization, some experimental and analytical mode shapes of the modified structure are depicted in Fig. 14.

Table 5. Natural frequencies of modified structure obtained from test and FEM

Mode Number	FEM (Modified)	Hammer (Modified)
1	6.012	6.55
2	11.41	13.93
3	30.21	32.35
4	32.88	34.95
5	33.60	35.48
6	34.25	38.03
7	47.11	48.62
8	49.59	50.06
9	55.07	56.41
10	57.52	58.04

Archive of SID

www.SID.ir

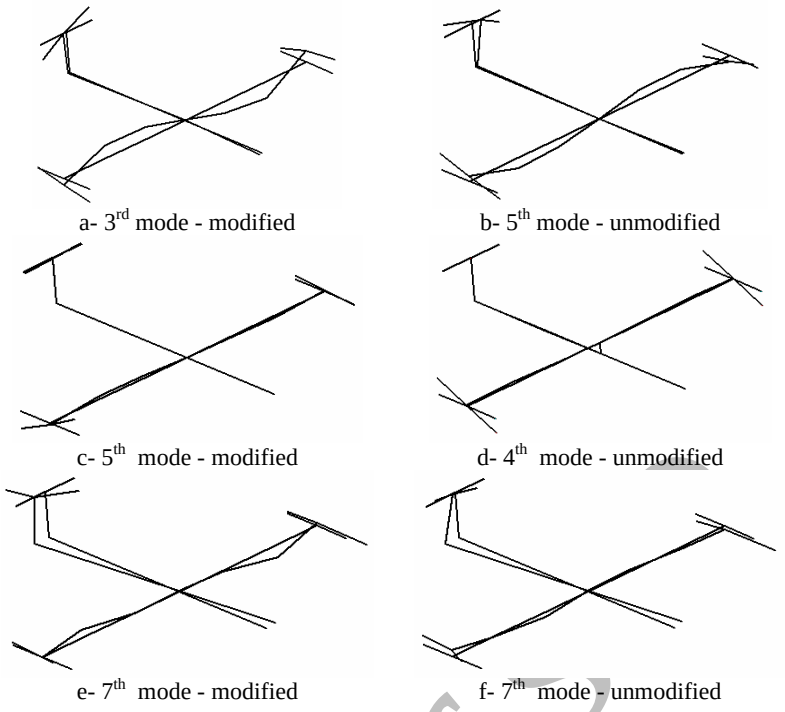

Fig. 14. Experimental mode shapes of the modified and unmodified structure

Figure 14 indicates that small changes in the symmetry of the structure cause essential changes in some of the mode shapes of the structure. Moreover, the unsymmetry changed the mode pairing. In order to find the new mode pairing between the modified and unmodified structure, correlation analysis was also carried out. The MAC values are calculated and plotted in Fig. 15. The correlated mode pairs are listed in Table 6. It can be seen that, for example, the sixth mode shape of the unsymmetric structure is correlated with the tenth mode of the symmetric structure. This means that the mode with a natural frequency of 69.68Hz (Table 3) in the symmetric structure correspond to the mode with a natural frequency of 38.03Hz (Table 5) in the unsymmetric structure. In other words, the natural frequency of some modes has shifted. It is noteworthy that such a change in vibration characteristics of any structure due to small unsymmetry is very important in the design of aircrafts.

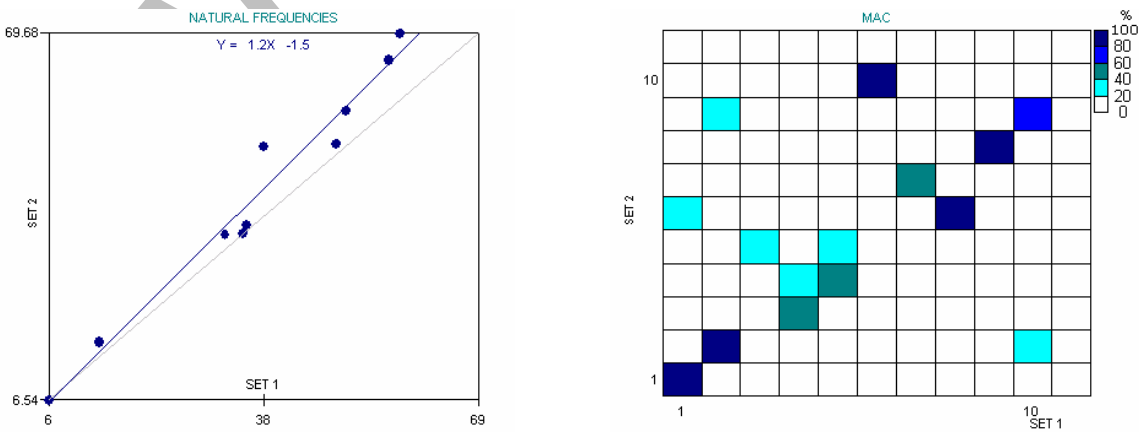

Fig. 15. MAC values of hammer test for modified and unmodified structures

www.SID.ir

Table 6. Modified and unmodified structure mode shape comparison

Modified structure (hammer)	Unmodified structure hammer or random()	Notes
1	1	-
2	2	Differences in wings end deflection
3	5	-
4	3	-
5	4	Differences in wings deflection
6	10	-
7	7	-
8	6	-
9	8	-
10	9	-

9. CONCLUSIONS

The authors performed a ground vibration test, modal parameter extraction, FE analysis and correlation analysis on an aircraft structure model. The test was carried out by hammer and shaker in a frequency range of 0 to 100Hz in free-free configuration and the first 10 elastic modes were extracted. A high correlation between various test excitations was achieved, confirming the accuracy of the experimental approach. Correlation between experimental and analytical modes, except for mode pairing, was fairly high indicating the FE model represents the dynamic behavior of the structure properly. Good correlation between phase resonance and phase separation test results demonstrates a high reliability on the applied technique.

A sine test with shaker was also conducted to recognize the close modes of the structure. Comparison between the results obtained from shaker and hammer recommends that the hammer test can accurately predict the close modes of the structure.

Correlation analysis between modified and unmodified structures was also investigated. It was shown that small changes in the symmetry of the structure can cause fundamental changes in mode pairing and mode shapes. Also, the change in symmetry can cause major shifts in some natural frequencies.

REFERENCES

1. Remmers, G. M. & Belsheim, R. O. (1964). Effects of technique on reliability of mechanical impedance measurement. *Shock and Vibration Bulletin, 34*(3).
2. Ewins, D. J. & Griffin, J. (1981). A state of the art assessment of mobility measurement techniques–results for the mid- range structures (30-3000Hz). *Journal of Sound and Vibration*, *78*(2), 197-222.
3. Balmes, E. (1998). Predicted variability and differences between tests of a single structure. IMAC XVI, Santa Barbara, CA, 558-564.
4. Degener, M. & Hermes, M. (1996). Ground vibration test and finite element analysis of the GARTEUR SM-AG19 testbed. DLR report.
5. Balmes, E. & Wright, J. (1997). GARTEUR Group on ground vibration testing results from the test of a single structure by 12 laboratories in Europe. *Proceeding of International Modal Analysis Conference*, Orlando.
6. Goge, D. & Link, M. (2003). Results obtained by minimizing natural frequency and mode shape errors of a beam model. *Mechanical Systems and Signal Processing*, *17*(1), 21-27.
7. Mares, C., Mottershead, J. E. & Friswell, M. I. (2003). Results obtained by minimizing natural frequency errors and using physical reasoning. *Mechanical Systems and Signal Processing*, *17*(1), 39-46.

Archive of SID

www.SID.ir

8. Bohle, K. & Fritzen, C. (2003). Results obtained by minimizing natural frequency and MAC value errors of a plate model. *Mechanical Systems and Signal Processing, 17*(1), 55-64.
9. Thonon, C. & Golinval, G. (2003). Results obtained by minimizing natural frequency and mac value errors of a beam model. *Mechanical Systems and Signal Processing, 17*(1), 65-72.
10. D'Ambrogio, W. & Fregolent, A. (2003). Results obtained by minimizing natural frequency and antiresonance errors of a beam model. *Mechanical Systems and Signal Processing, 17*(1), 29-37.
11. Ziaei-Rad, S. (2005). Finite element, modal testing and modal analysis of a radial flow impeller. *Iranian Journal of Science and Technology, Transaction B: Engineering, 29*(B2), 157-169.
12. Ziaei-Rad, S. (2005). Finite element model updating of rotating structures using different optimization techniques. *Iranian Journal of Science and Technology, Transaction B: Engineering, 29*(B6), 569-585.
13. Balmes, E., Chapelier, C., Lubrina, P. & Fargette, P. (1995). An evaluation of modal testing results based on the force appropriation method. *Proceedings of the 13th International Modal Analysis Conference*, Nashville, Tennessee, 47-53.
14. Ewins, D. J. (2000). *Modal testing: Theory, practice and application*. Second Edition, Research Studies Press.
15. Zaveri, K. & Phil, M. (1985). *Modal analysis of large structures-multiple exciter systems*. B&K press.

Archive of SID

www.SID.ir